Formation of highly oriented nanopores via crystallization of amorphous Nb_20_5 and Ta_20_5

doi: 10.1063/1.4822300

JOURNAL OF APPLIED PHYSICS **114**, 124308 (2013)

Formation of highly oriented nanopores via crystallization of amorphous Nb_2O_5 and Ta_2O_5

R. Nakamura,[1,a)] M. Ishimaru,[2] K. Sato,[3] K. Tanaka,[4] H. Nakajima,[5] and T. J. Konno[3]
[1]*Department of Materials Science, Graduate School of Engineering, Osaka Prefecture University, Gakuen-cho 1-1, Naka-ku, Sakai 599-8531, Japan*
[2]*Department of Materials Science and Engineering, Kyushu Institute of Technology, Tobata, Kitakyushu, Fukuoka 804-8550, Japan*
[3]*Institute for Materials Research, Tohoku University, Katahira 2-1-1, Sendai 980-8577, Japan*
[4]*The Institute of Scientific and Industrial Research, Osaka University, Mihogaoka 8-1, Ibaraki, Osaka 567-0047, Japan*
[5]*The Wakasa Wan Energy Research Center, Tsuruga, Fukui 914-0192, Japan*

(Received 5 August 2013; accepted 9 September 2013; published online 25 September 2013)

Formation of self-oriented and -elongated nanopores in annealed amorphous Nb_2O_5 and Ta_2O_5 was analyzed by transmission electron microscopy. Along with their crystal growth, nanopores were spontaneously elongated in the *a*-axis direction perpendicular to the longitudinal *b* axis of the orthorhombic structures with strong anisotropy. In addition, the effect of tungsten on the nanovoid formation in annealed amorphous Nb_2O_5 and Ta_2O_5 was also studied. Additive tungsten atoms of a few atomic percent into Nb_2O_5 and Ta_2O_5 were found to make the aspect ratio of nanopores larger. Electron diffraction experiments revealed that the crystallized regions including elongated nanopores possess a variety of periodicity in the *b*-axis direction. This structural flexibility in the crystal growth of strong anisotropic structures seems to play an important role on the unidirectional growth of nanopores. © *2013 AIP Publishing LLC*. [http://dx.doi.org/10.1063/1.4822300]

INTRODUCTION

Porous oxides have attracted extensive attention as functional materials in categories such as ion exchange, molecular separation, catalysis, chromatography, and energy storage, because their properties can be vastly improved by increasing the surface-to-volume ratio.[1,2] Typical nanoporous oxides, such as mesoporous silica[3] and transition metal oxides,[4] are fabricated by chemical synthesis routes which combine the use of a template and an etching process. Such chemical synthesis techniques are based on the concept of creating spaces by eliminating the nano-sized templates. In our research, on the other hand, a bottom-up technique to produce nanoporous structures through the accumulation of atomic level spaces is employed. Amorphous Al_2O_3 (a-Al_2O_3), WO_3 (a-WO_3), and Ta_2O_5 (a-Ta_2O_5) were found to become nanoporous structures as a result of structural change and crystallization by annealing in air.[5,6] The evolution of nanopores originates in the accumulation of amounts of atomic level spaces existing at loosely bonded regions of the amorphous oxides, whose densities are 20%–30% lower than those of their counterpart crystalline phases.

Among the oxides described above, Ta_2O_5 exhibits a unique pore-formation behavior.[6] Highly oriented and elongated nanopores are spontaneously formed along with the crystallization into orthorhombic β-Ta_2O_5, whose unit cell ($a = 0.389$ nm, $b = 4.029$ nm, $c = 0.620$ nm (Ref. 7)) is strongly anisotropic. The pores are elongated in the *a*-axis direction perpendicular to the longitudinal *b* axis of the orthorhombic structure. The finding raises the possibility of fabricating highly ordered nanoporous transition-metal oxides of not only Ta_2O_5 but also Nb_2O_5, whose orthorhombic structure is also strongly isotropic.[8] Fabrication of such highly oriented nanoporous Ta_2O_5 and Nb_2O_5 enables the application as electronics and sensor devices to expand considerably. For example, the dielectric property of Ta_2O_5 (Ref. 9) and the power conversion efficiency of Nb_2O_5 as a dye-sensitized solar cell material[10] can be improved by providing large surface areas in order to increase high specific charge and electron diffusion length. Therefore, for the better understanding of the formation mechanisms of self-oriented nanopores, comprehensive studies for Nb_2O_5 as well as Ta_2O_5 are required. The first purpose of the present work is to characterize the formation behavior of nanopores in annealed amorphous Nb_2O_5 by transmission electron microscopy (TEM).

The self-organization of nanopores by the present technique, as mentioned above, originates in the structural features of amorphous and crystalline matrices and in dynamic behavior during structural changes towards crystallization, suggesting that the properties of nanopores such as size, density, or morphology are expected to be manipulated by modifying amorphous and/or crystalline microstructures. One of the possible routes for the purpose must be to introduce additive elements. In a previous work,[11] we examined the effect of a third element, tungsten, on the pore formation in a-Al_2O_3. The addition of tungsten into a-Al_2O_3 is effective for inducing larger and denser pores than in a-Al_2O_3 without tungsten. The enhancement of pore formation is due to the structural change of a-Al_2O_3; the introduction of tungsten atoms makes amorphous structure more disordered, resulting in the decrease in density, i.e., the increase in atomic level

[a)]E-mail: nakamura@mtr.osakafu-u.ac.jp

spaces. The effect of tungsten on the pore formation behavior in Nb_2O_5 and Ta_2O_5 must be clarified from a scientific perspective and also in terms of the potential applications of these materials. In the present work, the formation behavior of nanopores in annealed amorphous Nb_2O_5 and Ta_2O_5 containing tungsten atoms was also examined by analyzing the atomic structure of the amorphous oxides in terms of pair distribution function (PDF) and the crystallographic properties after annealing by TEM.

EXPERIMENTAL PROCEDURE

Thin films of amorphous Nb_2O_5 (a-Nb_2O_5) and Ta_2O_5 (a-Ta_2O_5) were prepared by radio-frequency sputtering a crystalline oxide target with 99.9% purity. Resistive heating deposition was also used for preparing a-Nb_2O_5 and a-Ta_2O_5 thin films including tungsten, the concentration of which was aimed for a few at. %. In evaporating a grain of the oxides on a tungsten coil as a heating source, tungsten is inevitably introduced into the deposited oxide films.[11] A cleavage NaCl crystal was used as the substrate. The NaCl on which the 15–30 nm thick oxide thin film was deposited was put into distilled water, and then the floating thin film was mounted onto a platinum grid. The amorphous oxide on the Pt grid was subjected to heat-treatment in an electric furnace in air at 773–1023 K for 1 h. Some of the crystallized specimens after annealing were coated with carbon to reduce the effects of charging at TEM observations.

The changes in its morphology and structure were examined by a Hitachi H-800 type TEM and a JEOL JEM-3000F TEM at 300 kV. Atomic number contrast (Z-contrast) images of scanning TEM (STEM) were obtained using a FEI Titan 80-300 TEM operating at 300 kV with a high-angle annular dark-field (HAADF) detector. The tilt series of Z-contrast images were acquired within the detector angle between 60 and 210 mrad, and 3D reconstruction was performed by using the INSPECT3D software package (FEI Co. Ltd). The intensities of selected-area electron diffraction (SAED) patterns were recorded on an imaging plate (Eu^{2+} doped BaFBr). To avoid contamination, in particular, electron diffraction intensities for PDF analysis were measured at cryogenic temperature using a cooling holder. The intensities of halo-patterns from the as-deposited amorphous samples were analyzed quantitatively using a Digital Micro-Luminography FDL5000.[12,13] The composition was analyzed by the TEMs equipped with an energy dispersive X-ray spectrometer (EDS).

RESULTS AND DISCUSSION

Figure 1 shows a typical change in structure and morphology during the annealing of amorphous Nb_2O_5 (a-Nb_2O_5) prepared by sputtering. As shown in the bright field image (BFI) of Fig. 1(a), no void-contrast can be detected in an as-deposited thin film of a-Nb_2O_5. On the other hand, a high density of spherical nanopores with an average diameter around 3 nm appears in a-Nb_2O_5 annealed at 773 K (b). The structure of thin films remains amorphous up to 773 K at an annealing time of 1 h while crystallized regions appear in the amorphous matrix at 823 K for 1 h, as can be seen in Fig. 1(c). In the amorphous region of (c), a number of spherical nanopores can be seen, as is the case with at 773 K. On the other hand, pores in the crystallized region show a tendency to aggregate and grow larger than those in the amorphous region. It is particularly noteworthy that the pores near the front of interface of the crystallized phase tend to be elongated. As a result of crystallization at a high temperature of 923 K, self-elongated and oriented nanopores are formed (d).

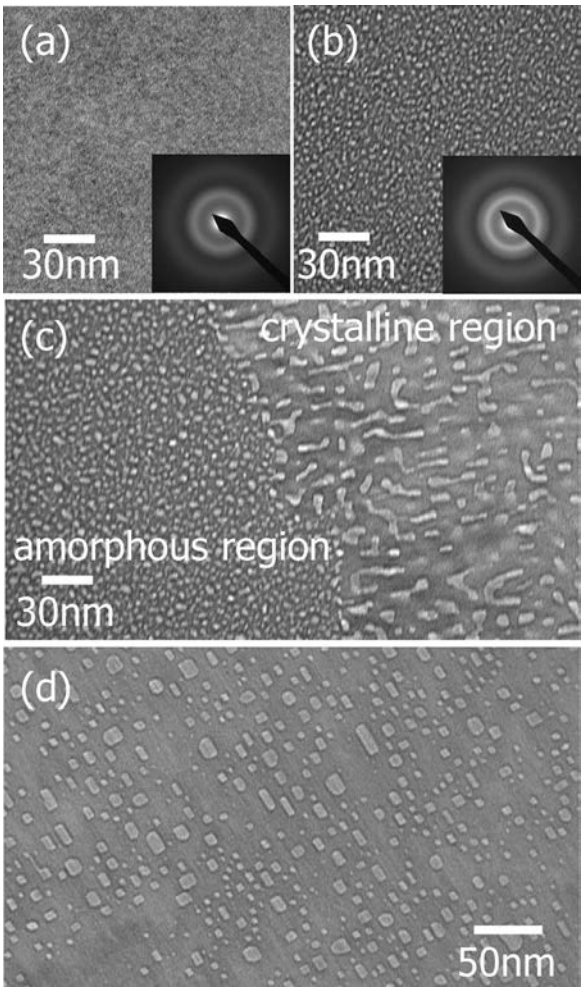

FIG. 1. A typical example of changes in morphology and structure of a-Nb_2O_5 during annealing in air: (a) as-deposited, (b) 773 K, (c) 823 K, and (d) 923 K for 1 h.

Figure 2 shows the BFIs (a) and SAED patterns (b) of fully crystallized Nb_2O_5 films, after annealing at 873 K for 1 h, where an array of elongated nanopores appears. The beam incidence is to [014] direction. The structure of crystallized Nb_2O_5 was identified as orthorhombic Nb_2O_5 ($a = 0.392$ nm, $b = 4.379$ nm, $c = 0.624$ nm (Ref. 8)). The electron diffraction patterns (c), simulated on the basis of the orthorhombic structure model (c′), conform to the experimentally obtained diffraction patterns (b). The direction of elongated pores is parallel to the *a* axis, and therefore, perpendicular to the longitudinal *b* axis of the orthorhombic structure. The relationship between pore and crystal orientations in orthorhombic Nb_2O_5 is in good agreement with that in orthorhombic Ta_2O_5,[6] indicating that the formation of the self-organized nanopores can be attributed to the strong

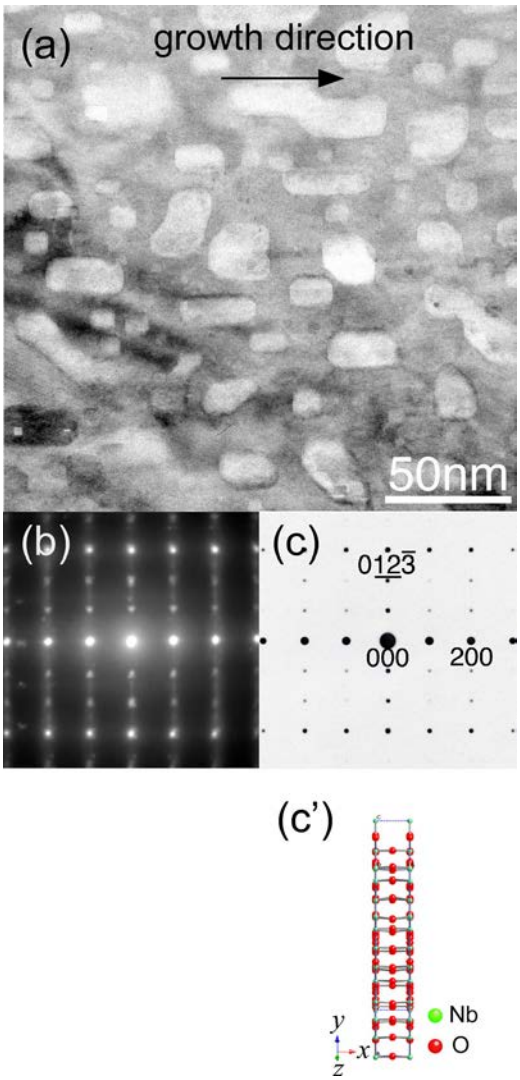

FIG. 2. BFI (a) and SAED patterns (b) of the fully crystallized Nb_2O_5 film after annealing at 873 K for 1 h. The *c*-axis is almost perpendicular to the photograph. (c) Electron diffraction patterns simulated from the structure model of orthorhombic Nb_2O_5 (c′).

anisotropy of orthorhombic structure of the pentoxides. A proposed mechanism is corporative growth of pores along with crystalline phase in the amorphous matrix.[6] The growth of the (100) plane is limited due to the long periodic structure of the β-Ta_2O_5 unit along the *b*-axis direction; the atomic arrangement towards the long-periodic *b*-axis in the (100) plane is more difficult than the *a*- and *c*-axes. The strong isotropic nature of Nb_2O_5 as well as Ta_2O_5 allows for the faceted and slow growth of (001) plane, which provides the growing nanopores with enough time to absorb free volume as well as existing nanopores at the boundary between amorphous and crystalline phases as crystal growth occurs. As a result, nanopores show a tendency to grow unidirectionally.

Figure 3 shows a low-energy portion of energy-dispersive X-ray spectra of as-deposited a-Nb_2O_5 (a) and a-Ta_2O_5 (b), prepared by resistive heating deposition. The characteristic X-rays of Pt in a-Ta_2O_5 (b) come from the grid. The W M and L peaks are observed in both oxides. As is the case with resistive heating deposition of Al_2O_3,[11] tungsten is self-evaporated into the Nb_2O_5 and Ta_2O_5 thin films from a tungsten coil used as a

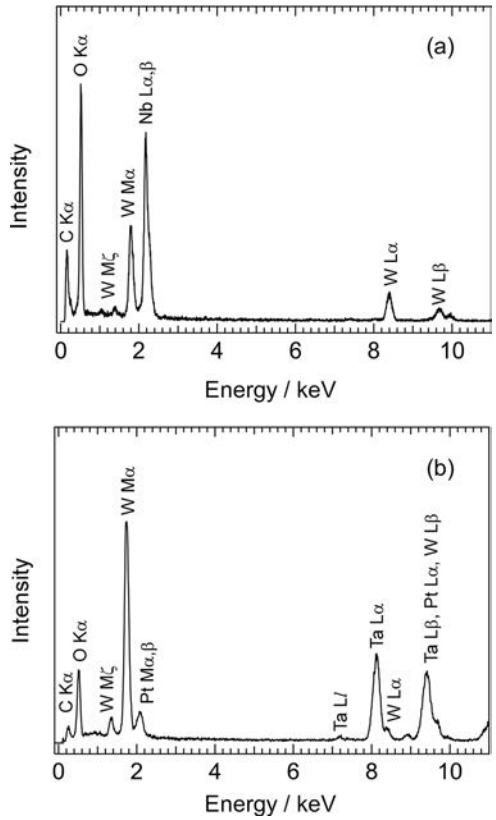

FIG. 3. Energy-dispersive X-ray spectra of as-deposited amorphous (a) Nb_2O_5-W and (b) Ta_2O_5-W.

heating source. Although it is hard to determine precisely the concentration of tungsten because of large difference in atomic number between metal and oxygen ions, the concentration of W is probably around 5 at. % in a-Nb_2O_5-W and 2 at. % in Ta_2O_5-W. Hereafter, the samples are denoted as Nb_2O_5-W and Ta_2O_5-W. Figures 4(a)–4(d) show the BFIs of amorphous Nb_2O_5-W and Ta_2O_5-W after annealing at 823–973 K for 1 h. It was found that a large amount of spherical nanopores around 3 nm is formed in the a-Nb_2O_5-W annealed at 823 K (a) and a-Ta_2O_5-W at 923 K (c) and then they grow into elongated and oriented shapes after crystallization at 873 K (b) and 973 K (d). The overall picture of pore formation behavior in Nb_2O_5-W and Ta_2O_5-W is consistent with that of Nb_2O_5 (Figs. 1 and 2) and Ta_2O_5 (Ref. 6) without W, prepared by sputtering. Figure 4(e) shows the high-resolution TEM image of crystallized Ta_2O_5-W and its Fourier power spectrum. The bright domains correspond to less densely regions, i.e., nanopores, and they elongate along the horizontal direction. The spectrum is consistent with the (001) electron diffraction pattern (cf. the diffraction pattern of Figs. 7 and 8). Again, it was confirmed that the nanopores elongate in the *a*-axis direction perpendicular to the longitudinal *b* axis of the orthorhombic structures. However, a different feature of pore formation can be recognized: the pores in the oxides with W have higher aspect ratio than those in the oxides without W. The comparison in reconstructed 3D image between fully crystallized Ta_2O_5-W and Ta_2O_5,[6] shown in Fig. 5, reveals clearly that the elongation of nanopores toward the preferential *a*-axis direction in Ta_2O_5-W is more pronounced compared to that in Ta_2O_5 without W.

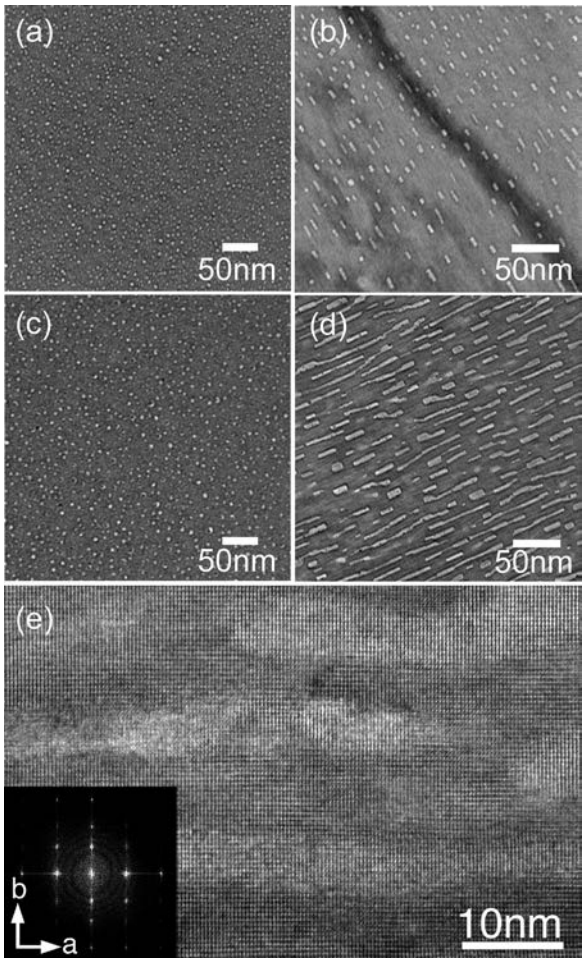

FIG. 4. BFIs of amorphous Nb_2O_5 and Ta_2O_5 containing W after annealing in air for 1 h: (a) at 823 K and (b) 873 K for Nb_2O_5-W, and (c) at 923 K and (d) 973 K for Ta_2O_5-W. (e) A high-resolution TEM image of crystallized Ta_2O_5-W and its Fourier power spectrum.

To discuss the effect of W on the pore formation behavior, we performed two types of analyses from the viewpoint of structural properties: one is pair distribution analysis of the amorphous oxides with and without W and the other is the comparison of lattice spacing between the crystalline oxides. Figures 6(a) and 6(b) show the atomic PDF of

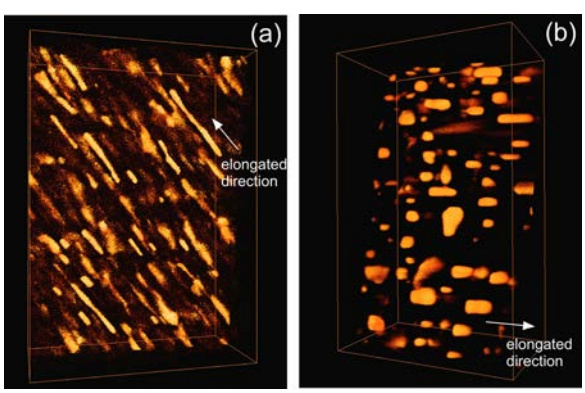

FIG. 5. Reconstructed 3D images of elongated nanopores included in the crystallized Ta_2O_5-W at 973 K (a) and Ta_2O_5 at 1023 K (b) observed by HAADF-STEM tomography. The size of reconstructed region of (a) and (b) is 209 nm × 295 nm × 98 nm and 115 nm × 189 nm × 74 nm, respectively.

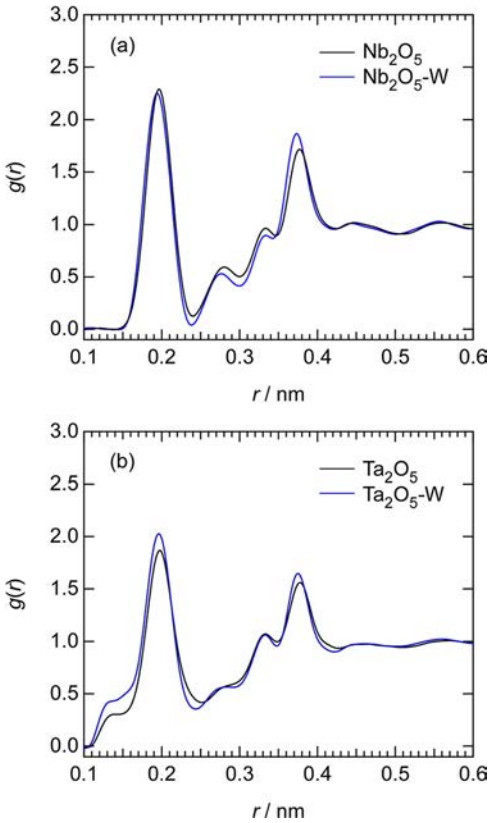

FIG. 6. Atomic pair distribution function $g(r)$ of as-deposited amorphous Nb_2O_5 (a) and Ta_2O_5 (b) with and without tungsten atoms.

as-deposited a-Nb_2O_5 and a-Ta_2O_5 with and without W. The PDF was obtained by analyzing the SAED patterns taken from the region of 300 nm in diameter. The detailed procedures of RDF analysis using electron diffraction techniques are described elsewhere.[12,13] Both amorphous oxides have similar atomic-bond properties: the first and second peaks corresponding to Nb(or Ta)-O and O-O are located around 0.20 nm and 0.28 nm, respectively, and the double peaks for Nb-Nb (or Ta-Ta) around 0.33 and 0.38 nm. The atomic distribution in a-Ta_2O_5 is almost consistent with that reported by Bassiri *et al.*[14] The peak position and intensity of the PDF for a-Nb_2O_5 and a-Ta_2O_5 agree well with those of a-Nb_2O_5-W and a-Ta_2O_5-W, even though there is somewhat discrepancy in film thickness due to different sample preparation processes. Therefore, the addition of W into the oxides induces no remarkable change in amorphous structure, which is different clearly from the effect of W on the structure of a-Al_2O_3.[11] The short-range atomic configurations of amorphous Al_2O_3 containing W are similar to those of a pseudo-liquid state, which is more disordered and has a lower density (larger atomic level spaces) than the amorphous solids, resulting in the enhancement of pore formation.[11] It seems that the difference in the effect of W on the amorphous structure of these oxides arises from the conformity of ionic properties in the matrices. In Al_2O_3, the introduction of W must disorder the state of coordination and bond-length in amorphous Al_2O_3 because the higher valence of W^{5+} or W^{6+} cations attract O^{2-} ions rather than lower valence Al^{3+} cations. On the other hand, the charge state of W is close to that for

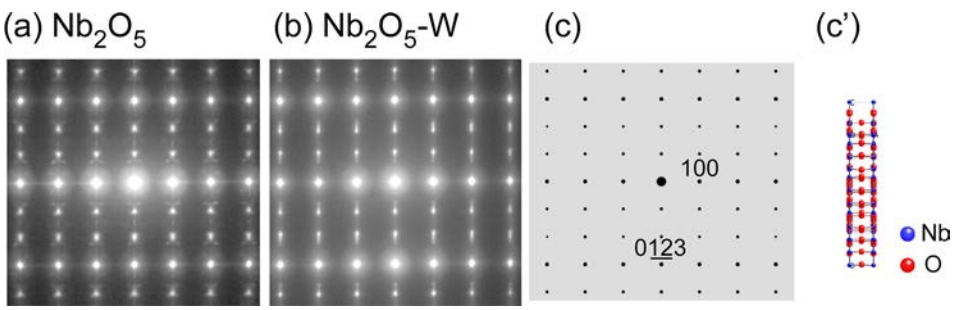

FIG. 7. Comparison of SAED patterns of fully crystallized Nb_2O_5 with (a) and without (b) tungsten atoms. The direction of incident electron beam is [014]. (c) Electron diffraction patterns simulated from the structure model of orthorhombic Nb_2O_5 (c′).

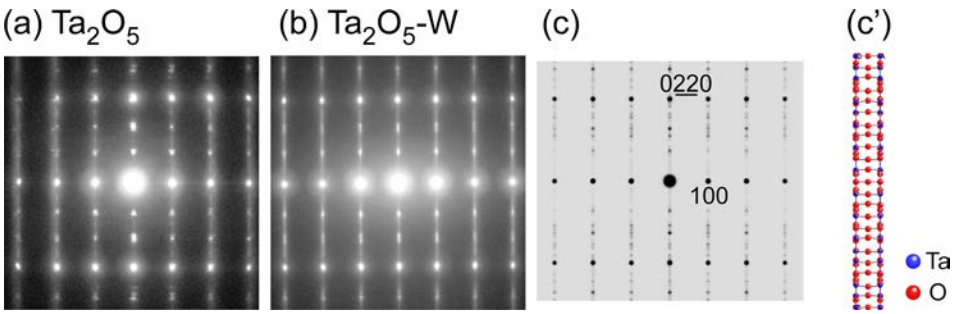

FIG. 8. Comparison of SAED patterns of fully crystallized Ta_2O_5 with (a) and without (b) tungsten atoms. The direction of incident electron beam is [001]. (c) Electron diffraction patterns simulated from the structure model of orthorhombic Ta_2O_5 (c′).

Ta^{5+} and Nb^{5+} so that W atoms dissolve into amorphous Nb_2O_5 and Ta_2O_5 with the short-range order being maintained.

Figures 7 and 8 compare the SAED patterns of pentoxides with and without W after the full crystallization. The beam incidence was identically set to be in the [014] for Nb_2O_5 (Fig. 7) and [001] for Ta_2O_5 (Fig. 8), respectively. The experimentally obtained SAED patterns ((a) and (b)) are in good agreement with the diffraction patterns (c), simulated from the orthorhombic models (c′). The spacing of fundamental and superlattice reflections of Nb_2O_5 and Ta_2O_5 is almost consistent with that of Nb_2O_5-W and Ta_2O_5-W, indicating that the lattice spacing of the basic unit cell and the periodicity in the direction of longitudinal *b*-axis of orthorhombic structures are maintained in spite of the introduction of W. Here, periodicity represents superstructures along [010] with multiplicities (*m*) of the unit length of *b*-axis of the substructure (e.g., $a = 0.389\,\text{nm}$, $b = 0.366\,\text{nm}$, $c = 0.620\,\text{nm}$ for Ta_2O_5 (Refs. 15 and 16)).

The fully crystallized samples contain partly the grains with spherical, non-oriented pores. Figure 9 compares a typical example of SAED patterns taken from the regions which contain oriented (a) and non-oriented (b) pores in Ta_2O_5-W. The streaks appear sharply from the oriented regions (see the inset of Fig. 9(a)), which can be attributed to a wide variety of periodicity in the *b*-axis direction. In the non-oriented regions (b), on the other hand, the streaks are very weak and the additional spots are scattered around the fundamental and superlattice reflections, indicating that the periodicity is not flexible but limited. These tendencies can be seen commonly in the oriented and non-oriented crystallized regions of Ta_2O_5, Nb_2O_5, and Nb_2O_5-W. In the oriented region, the atomic arrangement towards the long-periodic *b*-axis must occur variably during the crystal growth in the amorphous matrix. Under such a condition, pores are likely to grow smoothly in the elongated direction of *a*-axis along by absorbing atomic level spaces and existing spherical pores. As shown in Figs. 4 and 5, additive tungsten atoms enhance the self-elongation of pores. Stephenson and Roth[17–19] reported that the periodicity in the *b*-axis direction of orthorhombic Ta_2O_5 varies according to the concentration of tungsten: the value of multiplicities, *m*, is 8, 13, and 19 for $Ta_{30}W_2O_{81}$, $Ta_{22}W_4O_{67}$, and $Ta_{38}WO_{98}$, respectively. It is probable that solute tungsten atoms diffuse to be distributed to the forefront of growing crystalline phase at the amorphous-crystalline boundary, providing multiple periodicities and then higher variability of atomic arrangements during crystal growth. As a result, the elongation of pores with a larger aspect ratio is promoted by the addition of tungsten.

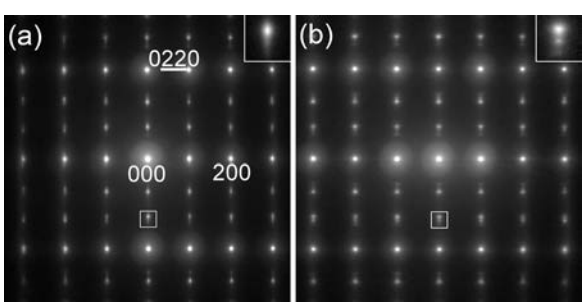

FIG. 9. Comparison of SAED patterns taken from the region including oriented pores (a) and non-oriented pores (b) in Ta_2O_5-W. A zoomed diffraction spot for enclosed point is at the upper-right corner.

In the preceding paper, a synergy effect between the strong isotropic structure and crystal growth has been considered to be important factors for the formation of oriented and elongated nanopores in Ta_2O_5.[6] Discussion on the latter effect, i.e., kinetic properties such as diffusion of components both at the surface and in the matrices is required to clarify deeply the effect of third element, tungsten, on the crystal and pore growth.

CONCLUSION

Self-oriented and -elongated growth of nanopores is induced as a result of crystallization of amorphous Nb_2O_5, as is the case with Ta_2O_5. The common feature of pore formation in niobium and tantalum pentoxides can be attributed to the strong isotropy of the orthorhombic structures. Electron diffraction analyses on the relationship between the long periodicity of orthorhombic structures and pore growth revealed that the variability of atomic arrangement in crystal growth must be a key factor enabling the unidirectional growth of nanopores.

It was found that the addition of third element, tungsten, into the oxides enhances the formation of nanopores with a higher aspect ratio. Both amorphous structure and crystallographic properties such as lattice constant and periodicity are maintained even by the addition of tungsten of a few at. % into Nb_2O_5 and Ta_2O_5. It seems that additive tungsten contributes to the change in the variability of atomic arrangement during crystal growth, resulting in the enhancement of unidirectional pore growth.

The results of present work suggest the possibilities of manipulating pore morphology by designing the additive elements into amorphous oxides. The highly oriented porous nanostructures are expected to enable the range of application of Nb_2O_5 and Ta_2O_5 to expand considerably: in the case of Nb_2O_5 to use as dye-sensitized solar cell materials,[10] and in the case of Ta_2O_5 to use as dielectric materials[9] and photocatalysis.[20] To obtain more highly ordered nanoporous structures, it may be worthwhile trying to control the crystal growth using external effects, e.g., under electric and magnetic fields, or on substrates with epitaxial relations.

ACKNOWLEDGMENTS

TEM observations were carried out at the Research Center for Ultra-High Voltage Electron Microscopy and the Comprehensive Analysis Center of ISIR, Osaka University. A portion of this study was performed under the inter-university cooperative research program of the IMR, Tohoku University. This work was supported by Grant-in-Aid for Young Scientists (B) (No. 24760574).

[1]C. T. Kresge, M. E. Leonowicz, W. J. Roth, J. C. Vartuli, and J. S. Beck, Nature **359**, 710 (1992).
[2]S. A. Johnson, P. J. Ollivier, and T. E. Mallouk, Science **283**, 963 (1999).
[3]Y. Wan and D. Zhao, Chem. Rev. **107**, 2821 (2007).
[4]J. Kondo, Y. Takahara, B. Lee, D. Lu, and K. Domen, Topics in Catalysis **19**, 171 (2002).
[5]R. Nakamura, T. Shudo, A. Hirata, M. Ishimaru, and H. Nakajima, Scr. Mater. **64**, 197 (2011).
[6]R. Nakamura, K. Tanaka, M. Ishimaru, K. Sato, T. J. Konno, and H. Nakajima, Scr. Mater. **66**, 182 (2012).
[7]R. S. Roth, J. L. Waring, and H. S. Parker, J. Solid State Chem. **2**, 445 (1970).
[8]R. A. Zvinchuk, Sov. Phys. Crystallogr. **3**, 750 (1960).
[9]I. Sieber, B. Kannan, and P. Schmuki, Electrochem. Solid-State Lett. **8**, J10 (2005).
[10]J. Z. Ou, R. A. Rani, M.-H. Ham, M. R. Field, Y. Zhang, H. Zheng, P. Reece, S. Zhuiykov, S. Sriram, M. Bhaskaran, R. B. Kaner, and K. Kalantar-zadeh, ACS Nano **6**, 4045 (2012).
[11]R. Nakamura, M. Ishimaru, A. Hirata, K. Sato, M. Tane, H. Kimizuka, T. Shudo, T. J. Konno, and H. Nakajima, J. Appl. Phys. **110**, 064324 (2011).
[12]T. Ohkubo and Y. Hirotsu, Phys. Rev. B **67**, 094201 (2003).
[13]M. Ishimaru, Nucl. Instrum. Methods Phys. Res. B **250**, 309 (2006).
[14]R. Bassiri, K. B. Borisenko, D. J. H. Cockayne, J. Hough, I. MacLaren, and S. Rowan, Appl. Phys. Lett. **98**, 031904 (2011).
[15]K. Lehovec, J. Less-Common Met. **7**, 397 (1964).
[16]I. E. Grey, W. G. Mumme, and R. S. Roth, J. Solid State Chem. **178**, 3308 (2005).
[17]N. C. Stephenson and R. S. Roth, Acta Crystallogr., Sect. B **27**, 1010 (1971).
[18]N. C. Stephenson and R. S. Roth, Acta Crystallogr., Sect. B **27**, 1018 (1971).
[19]N. C. Stephenson and R. S. Roth, Acta Crystallogr., Sect. B **27**, 1025 (1971).
[20]Y. Takahara, J. N. Kondo, T. Takata, D. Lu, and K. Domen, Chem. Mater. **13**, 1194 (2001).